Hydrodynamic and mass transfer parameters for CO2 absorption into amine solutions and its blend with nano heavy metal oxides using a bubble column

Hassan Pashaei, Ahad Ghaemi, Amir Hossein Behroozi & Hossein Mashhadimoslem

Published online: 17 May 2021.

Submit your article to this journal ⬈

Article views: 45

View related articles ⬈

View Crossmark data ⬈

ARTICLE

Check for updates

Hydrodynamic and mass transfer parameters for CO2 absorption into amine solutions and its blend with nano heavy metal oxides using a bubble column

Hassan Pashaei, Ahad Ghaemi ⓘ, Amir Hossein Behroozi, and Hossein Mashhadimoslem

School of Chemical, Petroleum and Gas Engineering, Iran University of Science and Technology, Tehran, Iran

ABSTRACT

In this work, hydrodynamic and mass transfer of CO_2 absorption into metal oxide nanofluid includes TiO_2, ZnO, and ZrO_2 nanoparticles at Piperazine (*Pz*) solution in the bubble column was studied. The novel rigorous correlations were extended based on the variable parameters for the calculation of gas holdup, enhancement factor, and mass transfer coefficients in the reactive absorption processes using the π-Buckingham method. The correlations were constructed based on dimensionless numbers, including nanoparticle loading, film parameter, CO_2 partial pressure ratio to the total pressure, the film thickness of phases, CO_2 loading, and ratio of diffusion coefficients of CO_2 in the gas and liquid phases. Experimental data were used to calculate the correlations, consisting of *Pz* concentration, CO_2 partial pressure, nanoparticle loading, and stirrer speed in the range of 0.1–0.5 mol/l, 16.0–35.2 kPa, 0.0–0.1 wt%, and 0–300 rpm, respectively. The film parameter was applied to exert the influence of chemical reactions on the performance of absorption. The mean squared error (R*MSEP*), the average absolute error (*%AARD*), and the coefficient of correlation of the results (R^2) for the correlations were in the range 0.021–2.604, 3.78–18.14, and 0.861–0.980, respectively, which represents the excellent accuracy of the proposed correlation.

Introduction

Greenhouse gases are intended as a significant origin for universal warming of the ground in recent years.[1–4] Among the greenhouse gases (GHG), carbon dioxide is the most significant contributor to global warming, and its uptake from the atmosphere is continuously affecting the earth's heat balance.[5–7] Environmental issues due to pollutant emissions from fossil fuel combustion have become global problems, [8] including air toxins and greenhouse gases. Further removal of acid gases, e.g., CO_2 and H_2S, from natural gas, which is known as natural gas sweetening process, is an essential part of refinery plants. The CO_2 removal may be utilized to enhance oil recovery, urea production, and beverage carbonation purposes.[5,9]

A wide variety of processes have been extended to remove acidic impurities from gas streams, such as adsorption, physical/chemical absorption, microbial fixation, membrane separation, and cryogenics separation.[10,11] Depending on the situation, each technology has its limitations, defects, applications, and benefits. Chemical absorption is one of the best methods in different industries, so experts pay more attention to it. This method has many advantages that distinguish it

from the methods. Low-pressure drop in comparison to solid adsorbents, simpler recovery process, and the possibility of increasing the efficiency by adding makeup to the treated absorbent continuously .[9,12]

Different types and solvent compounds have been investigated to trap carbon dioxide. The baseline solvent that has been applied for CO_2 capture is an aqueous monoethanolamine (*MEA*) solution. *MEA* is a corrosion inhibitor, but the mixture of CO_2 with *MEA* solution is corrosive. Furthermore, under the impression of some gases like NO_x, O_2, and SO_2, *MEA* foam consists of pollution and high temperature. This complicates the absorption/desorption process performance with aqueous amine solutions for large scale.[13–15]

To improve the process, it is significant to discover novel, further effective solvents. Applying concentrated *Pz* is a substitute to the *MEA*-based process. Using *Pz* solutions has several advantages over *MEA*, such as[16,17]: nearly double CO_2 absorption capacity, thermal stability up to a 150°C, oxidative degradation is much lower, and low solvent vapor pressure. Besides that, Piperazine is a secondary amine, so in the presence of O_2 it can react with NO_x to form nitrosamine derivatives. Recently, aqueous *Pz* solution due to

This article has been corrected with minor changes. These changes do not impact the academic content of the article.

Table 1. Literature review on CO_2 absorption performance by aqueous Pz solutions.

Experimental device	Pz concentration	Amine component	Pressure (kPa)	Temperature (K)	Ref.
Disk column	0.041–0.21 (M)	MDEA	-	303–343	[22]
A wetted-sphere	0.058, 0.115, and 0.233 (M)	AMP	-	303 and 313	[23]
Wetted wall column	0.6 and 0.2 (M)	-	-	298–333	[16]
Wetted wall column	0.6 (M)	MDEA	-	313–343	[19]
Wetted wall column	0–0.019 (M)	-	450–1200	298 and 333	[24]
Stirred cell	0.6–1.5 (M)	-	Up to 50	Low to moderate temperatures	[25]
Wetted wall contactor.	0.2–0.8 (M)	-	Up to 5	298–313	[26]
Wetted Wall Column	2–12 molality	-	-	303–333	[9]
Wetted Wall Column	0.2–1 (M)	-	-	298–331	[27]
Packed column	0.3–1.1 (M)	-	Up to 9.2	300–310	[3]
Pressure drop method	20 wt%	-	200 to 1000	313 and 333	[28]
Wetted Wall Column	0.025–0.1	-	Up to 690	313 and 333	[29]
Packed column	7 wt%	AMP	100–4000	303–318	[30]
Bubble column	0.1–0.5 (M)	-	101.325	295.15	This work

its unique characteristics as a suitable stand-alone solvent for CO_2 removal has been successfully determined in the literature.[16,18] So, based on all of these reasons, Piperazine is used instead of MEA in the current study.[19] The absorption procedure is paired with chemical reactions between the Pz and the acid gases. By the way, the carbon dioxide absorption by the Piperazine is the most critical method. Aqueous Pz solutions are primarily consumed for the capture of acid gases from refinery, natural, and synthetic gas industries.[20] However, most often the absorption is through Pz according to chemical solvents. The solvents expanding in these gas treatment processes are generally aqueous solutions of Pz .[21] A literature review on CO_2 absorption performance using aqueous Pz solutions is presented in Table 1.

In the present study, based on our previous work,[18,31] the capture of CO_2 by metal oxide nanofluids (TiO_2, ZnO, and ZrO_2) at Pz solution in the bubble column was investigated. In this work, rigorous correlations (general and accurate) are proposed to calculate the gas holdup, mass transfer coefficients (K_G, k_l, and k_g), and enhancement factor based on the π-Buckingham method. The correlations are appropriate to a wide range of operating conditions in all equipment of absorption. Besides, in the presented correlation, the influence of nanoparticle loading, film parameter, the ratio of CO_2 partial pressure to the total pressure, the film thickness of phases, CO_2 loading, and ratio of diffusion coefficients of CO_2 in gas and liquid phases were evaluated.
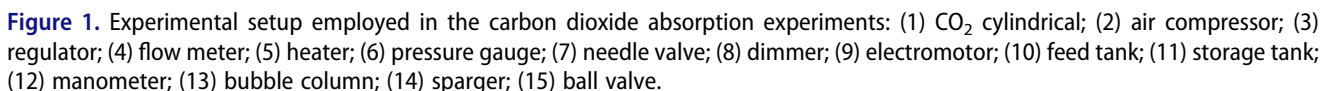
Experimental

Material

The nanofluids are produced with double-distilled water, Piperazine (Pz), and three TiO_2, ZnO, and ZrO_2 nanoparticles. Pz was provided by Sigma-Aldrich with a purity

of ≥99%. The CO_2 and air were introduced as a gas phase in the bubble column. The commercial grade of CO_2 gas with a minimum purity of 99.9% was introduced by Hor Mehr Tab Gas Co. and air was supplied from air compressor (AP-301, 300 l. Mahak Co.). The CO_2 and air gases were mixed in the mixing tank and adjusted to the required value with pre-calibrated flow meters and a temperature-controlled (22 ± 2)°C solution tank with an electric heater. The gas and liquid phases were operated in continuous mode.

Experimental set-up

The absorption process was performed using a stirrer bubble column experimental set-up, as shown in Fig. 1. The transparent glass with a specified surface area of 0.785 cm^2 was used to build the cylindrical column. The compressed air and CO_2 were transferred to a mixing tank from their cylinders. The desired values of CO_2 and air pressures were adjusted with separate regulators. Due to the high-pressure drop in the CO_2 tube, a heater was embedded before the regulator to eliminate the blocking phenomenon in the tube direction. The flow rate of the mixing gas was controlled with a flow meter, and needle valve and then it was sprayed into the bubble column. In order to generate the bubbles in the column, a stirrer with the sparger disc was utilized. The solution volume in the column was controlled with a manometer. All experiments were performed at ambient temperature. The outlet gas and solution flow rates were measured using two separate calibrated flow meters. The gas mixture was analyzed using a gas sensor Testo 327–1, Germany. The characteristics of used devices in the experimental set-up, material/physical properties, and operating conditions of this process are presented in Table 2. The measurement accuracy for pressure gauge, solution flow meter, gas flow meters, CO_2 analyzer, dimmer, and manometer, were ±0.1, ±0.1, ±0.01, ±0.001, ±1, and ±0.1, respectively.

Figure 1. Experimental setup employed in the carbon dioxide absorption experiments: (1) CO_2 cylindrical; (2) air compressor; (3) regulator; (4) flow meter; (5) heater; (6) pressure gauge; (7) needle valve; (8) dimmer; (9) electromotor; (10) feed tank; (11) storage tank; (12) manometer; (13) bubble column; (14) sparger; (15) ball valve.

Theory

Diffusion coefficient

The absorption of CO_2 into the amines is accompanied by the reaction, so the diffusion coefficient of CO_2 in aqueous amine solutions cannot be obtained directly. Therefore, these properties are evaluated using the N_2O analogy method as follows[32]:

$$D_{CO_2-amine} = D_{N_2O-amine}\left(\frac{D_{CO_2-water}}{D_{N_2O-water}}\right) \qquad (1)$$

D_{i-j} is the diffusion coefficient of i species into the j species. The diffusion coefficient of N_2O–H_2O and CO_2–H_2O as a function of temperature is as follows:

$$D_{N_2O-Water} = 9.72 \times 10^{-6} \exp\left(\frac{-2582}{T}\right) \qquad (2)$$

$$D_{CO_2-Water} = 8.13 \times 10^{-6} \exp\left(\frac{-2488}{T}\right) \qquad (3)$$

Diffusion coefficient of N_2O in aqueous Pz solution can be calculated by modified Stokes–Einstein equation[32]:

$$\left(\frac{D_{N_2O}\mu^{0.79}}{T}\right)_{Pz} = \left(\frac{D_{N_2O}\mu^{0.79}}{T}\right)_{Water} \qquad (4)$$

Loading (α)

The CO_2 loading (α) is defined as the absorbed CO_2 mole numbers relative to the number of absorbent moles as follows:

$$\alpha = \frac{n_{CO_2}}{\sum n_{Pz}} \qquad (5)$$

n_{CO_2} is the mole of absorbed CO_2 at each time step and n_{Pz} is the mole of Pz.

Film parameter (M)

The mass transfer is influenced by the chemical reaction, which is described by the film parameter (Hatta number). This parameter indicates as much as feasible alteration in the film relative to the maximum diffusional mass transfer among the film. All present CO_2 reactions in the system must be taken into account to define the film parameter. The reactions between CO_2 and Pz consist of Monocarbamate Pz hydrolysis with a mechanism of the second-order reaction rate.

$$M = \frac{\sqrt{k_{app}D_{CO_2-sol}}}{k_l} \qquad (6)$$

The method for calculating the apparent reaction rate constant has been given in our previous work,[33] which was obtained from the simultaneous solution of the equilibrium and reciprocal absorption reactions by considering pseudo-quadratic reactions. It should be noted that the above-mentioned equations (Eq. (1)-Ea. (6)) data calculated with ± 0. 1% accuracy.

Table 2. Characteristics of experimental set-up, material properties, and operational conditions of process.

Parameter		Parameter	
Material	Value	Operational conditions	Value
Air density (kg/m^3)	1.22	CO_2 flow rate (l/min)	1.0–2.2
CO_2 density (kg/m^3)	1.98	Air flow rate (l/min)	2.8–4.0
Water density (kg/m^3)	997.2	Stirrer speed (rpm)	0–300
Air viscosity (Pa.s)	1.983×10^{-5}	Pz	concentration (M) 0.1–0.5
CO_2 viscosity (Pa.s)	1.480×10^{-5}	Solution volume (l)	3
Water viscosity (Pa.s)	0.950×10^{-3}	nanoparticle loading (Wt %)	0.0–0.1
CO_2 diffusion coefficient in gas (m^2/s)	1.600×10^{-3}	Temperature (K)	295.15
CO_2 diffusion coefficient in water (m^2/s)	1.790×10^{-9}	Surface tension of solution (N/m)	0.06670–0.07148
Set-up dimension		**Stirrer properties**	
Column diameter (cm)	10	Company	-
Column height (cm)	50	Type	Disc
Diameter of distributor holes (mm)	1, 2 and 3	Material	Stainless steel
Distributer diameter (mm)	75	Plate diameter (mm)	80
Number of distributor holes (-)	1 and 6		

Buckingham π theorem

The Buckingham π is a theory to simplify a physical problem based on dimensional analysis, which decreases the number of relevant variables using dimensional homogeneity. The central premise of dimensional analysis is that the communication between the actual physical values remains valid in the physical equation form, which must be independent of the base units' magnitudes.[34] A complete set of independent variables must be identified that are probably to affect the physical value (Q_0), which is considered the dependent variable. The functional equation can be expressed as:

$$Q_1 = f(Q_2, Q_3, ..., Q_n) \quad (7)$$

The physical laws governing similar phenomena result in this equation. The dimension of each variable (Q_i) can be generally described by previously known primary dimensions. By considering length (L), mass (M), and time (t) as the primary dimensions, each variable can be written as:

$$[Q_i] = L^{l_i} M^{m_i} t^{\tau_i} \quad (8)$$

Where the exponents of l_i, m_i, and τ_i are dimensionless numbers. If the number of variables and primary dimensions in a problem being N and R, respectively, a group of $N − R$ equations can be described as the problem in the following form:

$$Q_{N-R} = \pi_{N-R}.Q_2^{a_{N-R}}.Q_3^{b_{N-R}}....Q_n^{m_{N-R}} \quad (9)$$

The corresponding problem can be described by this system of equations. The number of non-dimensional numbers ($i = N − R$), or independent dimensionless groups π, and arbitrary exponents of $a, b, ..., m$ can be determined. In the Buckingham π theorem, each group is connected to the others by a functional relationship as follows:

$$\pi_1 = f(\pi_2, \pi_3, ..., \pi_{N-R}) \quad (10)$$

The π theorem is a method to compute sets of dimensionless parameters from the identified parameters, and in general, it is a scheme for non dimensionalization. The Buckingham π theorem was used to obtain a specific relationship between the gas holdup, mass transfer coefficients, and enhancement factors. Based on this theorem, the gas holdup, mass transfer coefficients, and enhancement factor as a function of these factors are expressed in detail in Appendix A. In this work, liquid density, apparent gas velocity, and column diameter were used as repetitive variables on gas holdup and mass transfer. Besides, the diffusion coefficient, film thickness, and CO_2 concentration were used on the enhancement factor. Based on selected variables, the calculated dimensionless numbers for the gas holdup and another two-mass transfer coefficient, and enhancement factor are presented in Table 3.

Ultimately, the final dimensionless numbers for the gas holdup, mass transfer coefficients, and enhancement factor phenomenon are given in Appendix B in Table B.1. By substituting the experimental values, the gas holdup, mass transfer coefficients, and enhancement factor equations were determined using the data fitting method as for Eqs. (11)-(15):

$$\varepsilon_G = 2.3962 \times 10^{-5} \mathrm{Re}^{-0.07841} we^{-4.75251}$$
$$(\frac{u_g}{u_G})^{0.002252} (\frac{P_{CO_2}}{P_t})^{0.155541} (\frac{H_l}{D_c})^{0.012} \quad (11)$$
$$+ 7.04 \times 10^{-8} (\frac{D_c N}{u_G}) + 0.206(X)$$

Table 3. Dimensionless numbers obtained in CO_2 absorption process.

π-Groups		
Gas holdup	Mass transfer coefficient	Enhancement factor
$\pi_1 = \rho_G^x u_G^y D_c^z H_L$	$\pi_1 = \rho_G^x u_G^y D_c^z H_L$	$\pi_1 = D_{CO_2-Sol}^x \delta_l^y C_{CO_2}^z N_A$
$\pi_2 = \rho_G^x u_G^y D_c^z \mu_L$	$\pi_2 = \rho_G^x u_G^y D_c^z \mu_L$	$\pi_2 = D_{CO_2-Sol}^x \delta_l^y C_{CO_2}^z k_{app}$
$\pi_3 = \rho_G^x u_G^y D_c^z \sigma_L$	$\pi_3 = \rho_G^x u_G^y D_c^z \sigma_L$	$\pi_3 = D_{CO_2-Sol}^x \delta_l^y C_{CO_2}^z D_{CO_2-gas}$
$\pi_4 = \rho_G^x u_G^y D_c^z u_g$	$\pi_4 = \rho_G^x u_G^y D_c^z u_g$	$\pi_4 = D_{CO_2-Sol}^x \delta_l^y C_{CO_2}^z \delta_G$
$\pi_5 = \rho_G^x u_G^y D_c^z P_{CO_2}$	$\pi_5 = \rho_G^x u_G^y D_c^z P_{CO_2}$	$\pi_5 = D_{CO_2-Sol}^x \delta_l^y C_{CO_2}^z P_{CO_2}$
$\pi_6 = \rho_G^x u_G^y D_c^z P_t$	$\pi_6 = \rho_G^x u_G^y D_c^z P_t$	$\pi_6 = D_{CO_2-Sol}^x \delta_l^y C_{CO_2}^z P_t$
$\pi_7 = \rho_G^x u_G^y D_c^z N$	$\pi_7 = \rho_G^x u_G^y D_c^z N$	$\pi_7 = D_{CO_2-Sol}^x \delta_l^y C_{CO_2}^z C_{Pz}$
$\pi_8 = \rho_G^x u_G^y D_c^z X$	$\pi_8 = \rho_G^x u_G^y D_c^z X$	$\pi_8 = D_{CO_2-Sol}^x \delta_l^y C_{CO_2}^z N$
	$\pi_9 = \rho_G^x u_G^y D_c^z D_{CO_2-Sol}$	$\pi_9 = D_{CO_2-Sol}^x \delta_l^y C_{CO_2}^z X$

The dimensions of C_i, D_i, D_{i-j}, k_{app}, N, N_i, P_i, u_i, X, δ_i, and ρ_i are ML^{-3}, L, L^2T^{-1}, T^{-1}, T^{-1}, $ML^{-2}T^{-1}$, $ML^{-1}T^{-2}$, ML^{-1}, (-), ML^{-1}, and ML^{-3}, respectively.

$$K_G = 5.127 \times 10^{-5} \mathrm{Re}^{-0.09471} we^{0.04126}$$
$$\left(\frac{u_g}{u_G}\right)^{-0.02478} \left(\frac{P_{CO_2}}{P_t}\right)^{0.060279} \left(\frac{H_l}{D_c}\right)^{0.012} \times \left(\frac{D_{CO_2-sol}}{u_G D_c}\right)^{-0.0133}$$
$$- 1.81 \times 10^{-6} \left(\frac{D_c N}{u_G}\right)^{0.000331} - 2.326 \times 10^{-4}(X) \tag{12}$$

$$k_g = 4.814 \times 10^{-4} \mathrm{Re}^{-0.3471} we^{0.04126}$$
$$\left(\frac{u_g}{u_G}\right)^{-0.01478} \left(\frac{P_{CO_2}}{P_t}\right)^{-1.240279} \left(\frac{H_l}{D_c}\right)^{0.012} \times \left(\frac{D_{CO_2-sol}}{u_G D_c}\right)^{-0.0133}$$
$$- 1.3 \times 10^{-6} \left(\frac{D_c N}{u_G}\right)^{0.00311} - 2.326 \times 10^{-4}(X) \tag{13}$$

$$k_l = 5.167 \times 10^{-5} \mathrm{Re}^{-0.08671} we^{0.04126}$$
$$\left(\frac{u_g}{u_G}\right)^{-0.003442} \left(\frac{P_{CO_2}}{P_t}\right)^{-0.059279} \left(\frac{H_l}{D_c}\right)^{0.012}$$
$$\times \left(\frac{D_{CO_2-sol}}{u_G D_c}\right)^{-0.0133} - 1.81 \times 10^{-6} \left(\frac{D_c N}{u_G}\right)^{0.000331}$$
$$- 2.326 \times 10^{-4}(X)wt\%0.01 \tag{14}$$

$$E = 11.56 Sh^{0.9037} (\alpha)^{0.023} (M)^{-0.0102} \left(\frac{P_{CO_2}}{P_t}\right)^{-0.0356} \left(\frac{\delta_g}{\delta_l}\right)^{-0.0191}$$
$$\times \left(\frac{D_{CO_2-gas}}{D_{CO_2-sol}}\right)^{-0.5024} - 0.005\left(\frac{\delta_l^2 N}{D_{CO_2-sol}}\right) - 0.0009(X) \tag{15}$$

In order to calculate the error of obtained equations, Average Absolute Relative Deviation percentage (% AARD), Root Mean Square Error of Prediction (RMSEP), and Coefficient of correlation (R^2) are used, their formulas are presented below.

$$R^2 = \frac{\sum_{i=1}^{n} \left(Y_i^{\exp} - \overline{Y_i}\right)^2 - \sum_{i=1}^{n} \left(Y_i^{\exp} - Y_i^{cal}\right)^2}{\sum_{i=1}^{n} \left(Y_i^{\exp} - \overline{Y}\right)^2} \tag{16}$$

$$RMSEP = \sqrt{\frac{1}{n} \sum_{i=1}^{n} \left(Y_i^{\exp} - Y_i^{cal}\right)^2} \tag{17}$$

$$AARD\% = 100 \times \frac{1}{n} \sum_{i=1}^{n} \frac{\left|Y_i^{\exp} - Y_i^{cal}\right|}{Y_i^{\exp}} \tag{18}$$

where $Y_i^{\exp}$ and Y_i^{cal} indicate the experimental and predicted values by the presented correlations, respectively. n is the number of all sets of data and $\bar{Y}$ is the average of experimental values.

Result and discussion

Dimensional analysis and accuracy of correlations

As mentioned in the previous sections, the gas holdup, total mass transfer coefficient, enhancement factor, mass transfer coefficients in the gas, and liquid phases are correlated by fitting the experimental data. The *AARD*, RMSEP, and R^2 values are calculated for these correlations in Table 4. As can be seen, the minimum values of *AARD* and R*MSEP* are related to the enhancement factor and the mass transfer coefficient in the gas phase, respectively. Also, the correlation of k_g has the maximum R^2 relative to other correlations.

Gas holdup

Based on Buckingham π theorem, Eq. (11) is presented to calculate the gas holdup. This model can be used for various systems by correcting its constants. In this correlation, the effect of model parameters on the gas holdup is separately investigated. Fig. 2 shows the variations of the predicted gas holdup by the model against the experimental values in the *Pz* solution.

As can be observed in Fig. 2, the expanded correlation in the present study fitted well the experimental data with an *AARD* of 8.79%. Also, the predicted values for
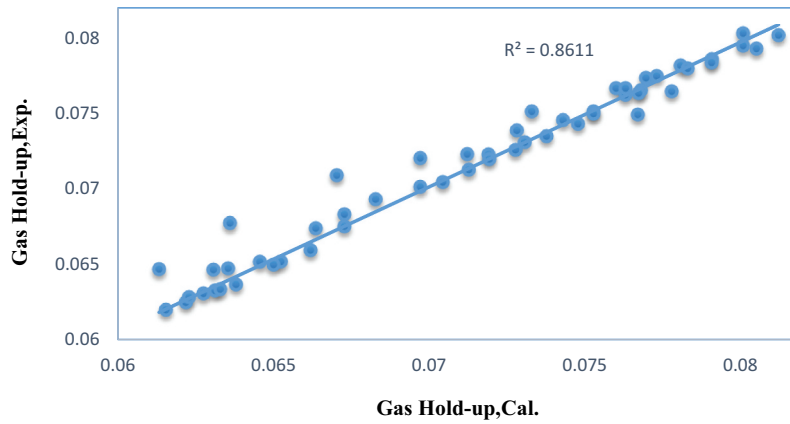
Fig. 2. Predicted gas hold-up versus experimental values using the Eq. (11) in the nanofluid.

the presented correlation are validated by the various studies as shown in Fig. 3.[35–39]

Mass transfer coefficients

Overall mass transfer coefficient

Fig. 4 depicts the model-based values for the total mass transfer coefficient versus experimental data. Also, from Fig. 5, the predicted total mass transfer coefficients are validated by experimental values from different studies.[40–42] In this figure, the solution flow rate and CO_2 partial pressure are 0.2 l/h and 28.8 kPa, respectively. It was considered that the quantities of the total mass transfer coefficient obtained from Li *et al*. and Liu *et al*. works are lower than those from the model presented in this study.

The effect of CO_2 concentration validation in 0.05 wt% of TiO_2 nanofluid at different Pz concentrations on the K_G value has been presented in Fig. 6.

The set-up pressure, nanofluid temperature, gas flow rate, and liquid flow rate are atmospheric, 295.15 K, 5.0 l/min, and 1.5 l/h, respectively. The results observed that the K_G is increased slightly with the CO_2 partial pressure. The identical conductance was distinguished by the increase in Pz loading as well, such that the K_G value changes with the Pz concentration. Based on the two-film theory, the resistance of the gas phase will decrease with the CO_2 partial pressure increase. Obviously, an increase in the CO_2 partial pressure, permits more CO_2 molecules to move from the gas bulk to the interface of the gas-liquid, leading to more mass transfer flux. With the mass transfer flux increase, the value of K_G increases accordingly as, by definition, mass transfer flux has a direct relation with K_G.

Mass transfer coefficient in the gas phase

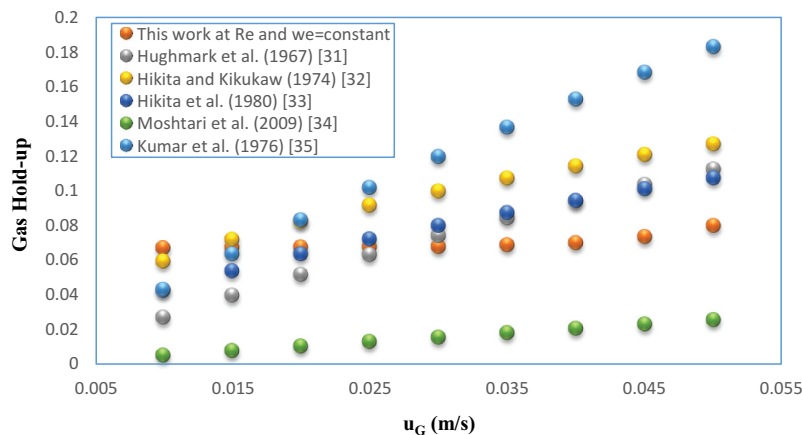Qualitative validation of the π-Buckingham model was performed based on comparison of the measured and

Fig. 3. Validation of present gas hold-up correlation with different empirical studies at different apparent gas velocities.
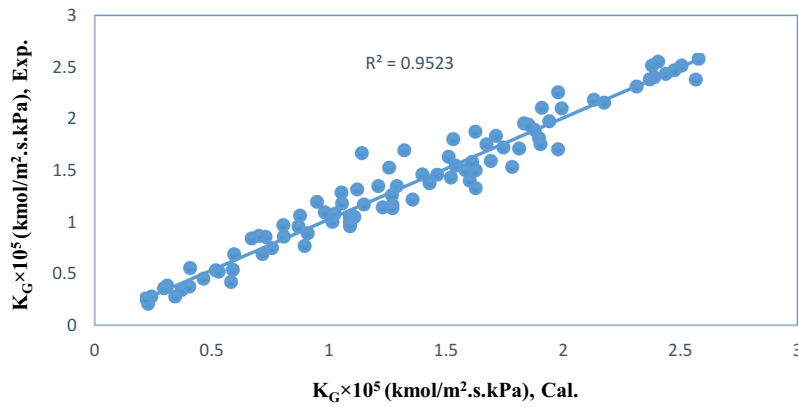
Fig. 4. Predicted total mass transfer coefficient from Eq. (12) versus experimental values in the nanofluid.
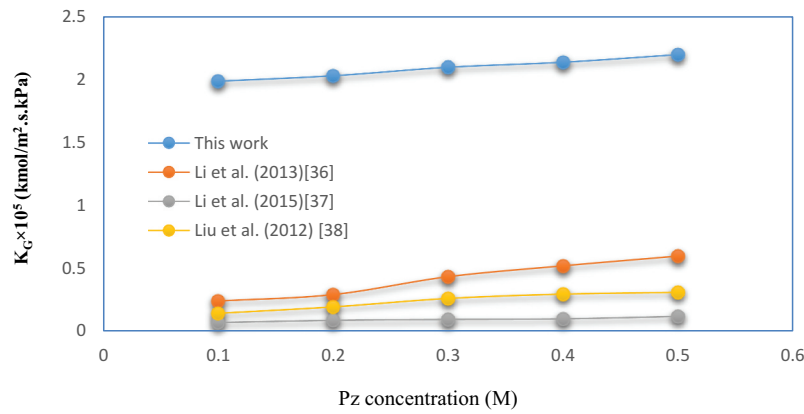

Fig. 5. Validation of the total mass transfer coefficient with different empirical studies at the various *Pz* concentrations.
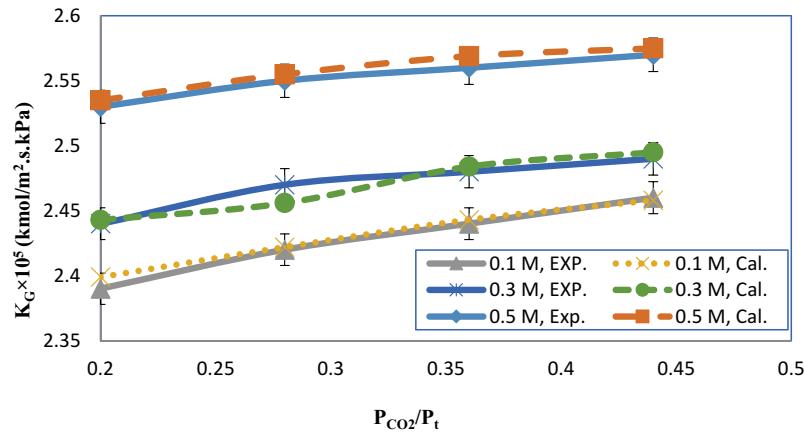

Fig. 6. Validation of the CO_2 partial pressure effects on the overall mass transfer coefficient using Eq. (12) and experimental data.

calculated values of k_g of the nanofluid. The calculations were performed for the same experimental operating parameters. The predicted and actual values for the mass transfer coefficient in the gas phase are shown in Fig. 7. As can be observed in this figure, the expanded correlation in the present study fits well with the experimental data with R^2 of 0.98. Also, the *Pz* concentration and flow rate of 0.5 M and 1.5 l/h are chosen to compare the k_g with the experimental data of Liu *et al.*[43] work in Fig. 8. They were studied the effect of some operating parameters on CO_2 absorption in
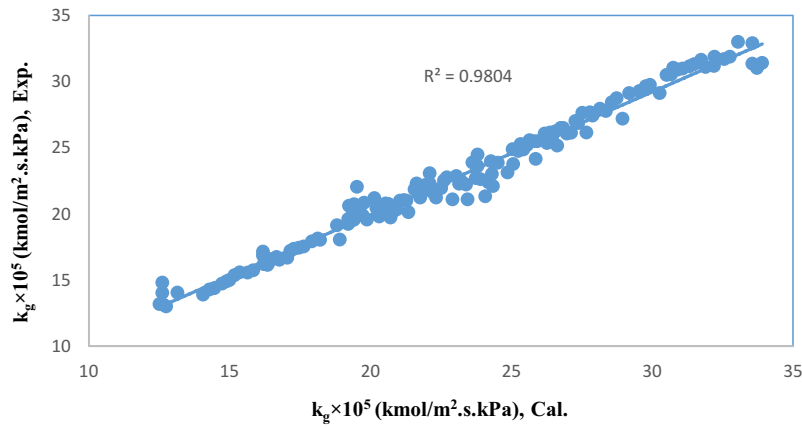
Fig. 7. Predicted mass transfer coefficient using Eq. (13) versus experimental values in the nanofluid.
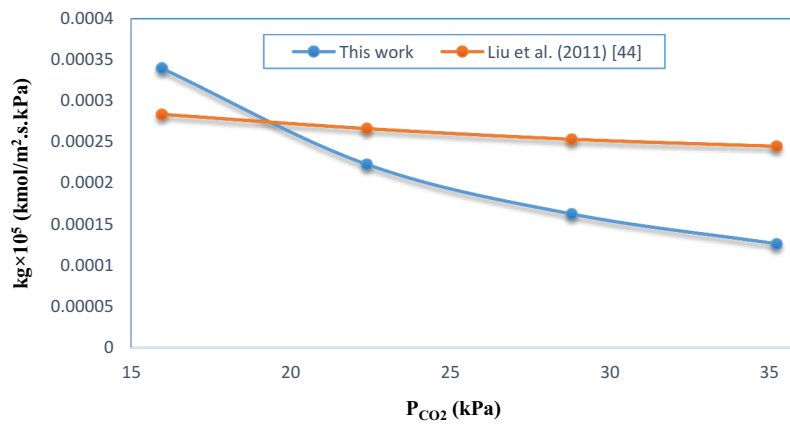

Fig. 8. Validation of mass transfer coefficient in the gas phase with Liu et al. empirical studies at various CO_2 partial pressures.
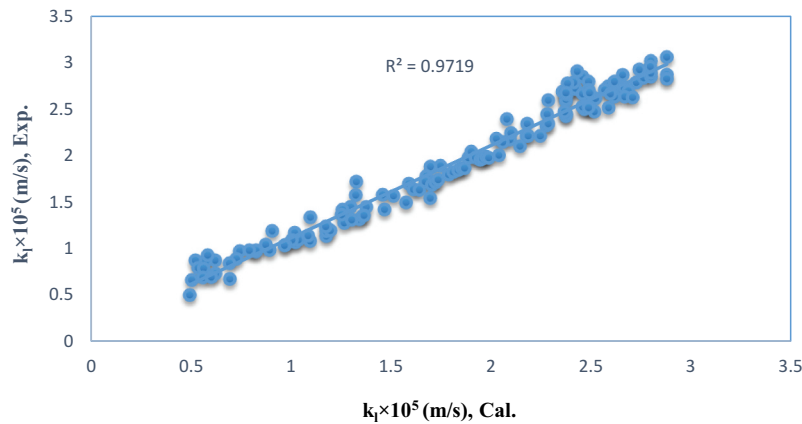

Fig. 9. The predicted mass transfer coefficient in the liquid phase from Eq. (14) versus experimental values in the nanofluid.

Pz solution by using a small wetted wall column (WWC). The experiments of CO_2 absorption into 0.1–0.4 M *Pz* at 10–40°C have been done under the driving force of 8–25 kPa in this paper. This figure is presented to evaluate and compare the gas side mass transfer coefficient obtained from the modeled data of the present work with Liu's work. As can see in this figure, there is a good fit between the two works (especially at CO_2 partial pressure of 20 kPa).

Mass transfer coefficient in the liquid phase

The predicted and empirical data for the mass transfer coefficient in the liquid phase are presented in Fig. 9.
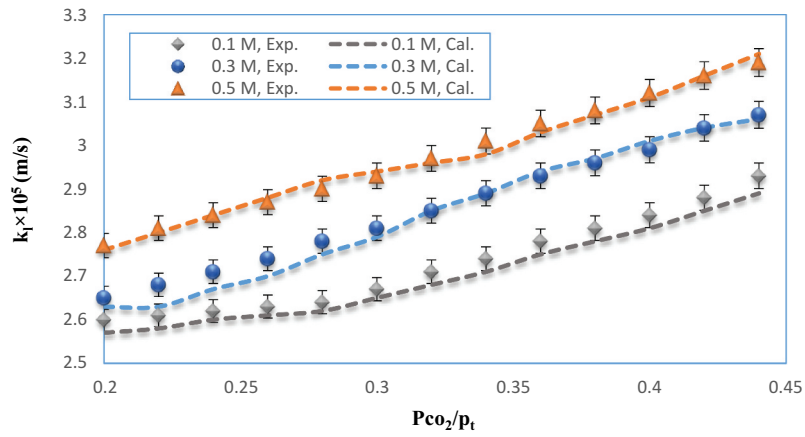
Fig. 10. Effects of *Pz* concentration on the predicted and empirical mass transfer coefficient in the liquid phase at the solution flow rate of 1.5 l/h.
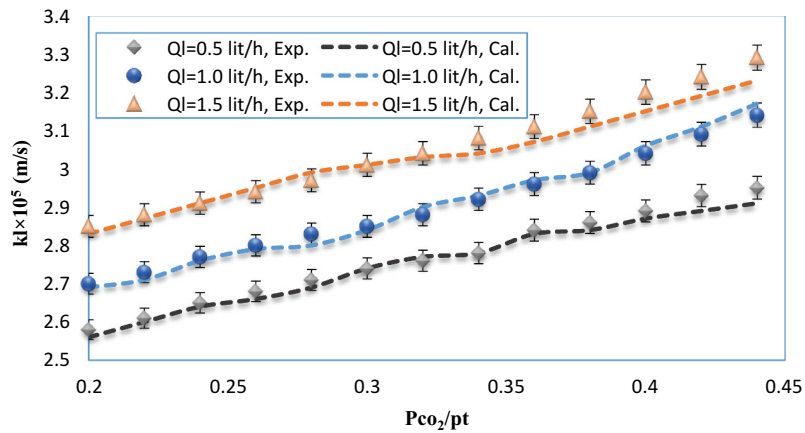

Fig. 11. Effects of solution flow rate on the predicted and empirical mass transfer coefficient in the liquid phase at the *Pz* concentration of 0.1 M.
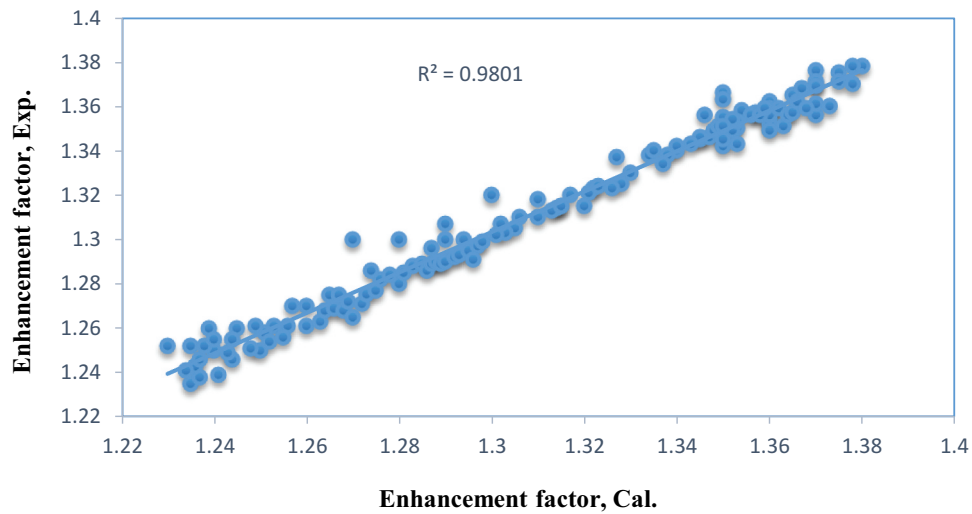

Fig. 12. The predicted enhancement factor from Eq. (15) versus experimental values in the nanofluid.

The affiliation of the mass transfer coefficient in the liquid phase on the CO_2 partial pressure is illustrated in Fig. 10 and Fig. 11. As the CO_2 partial pressure increases, the number of molecules present in the gas phase increases causing the mass transfer flux enhancement and consequently leading to an increase in the mass transfer coefficient. The mass transfer coefficient in the liquid phase at various Pz concentrations and constant solution flow rate is depicted in Fig. 10 and at various solution flow rates and constant Pz concentration in Fig. 11. As shown in these figures, an increase in CO_2 partial pressure causes increasing the mass transfer coefficient in the liquid phase.

Enhancement factor

The variation of the enhancement factor based on the presented correlation is shown versus experimental values in Fig. 12. The AARD was obtained 3.8% for the predicted values of the enhancement factor. The predicted values from Eq. (12) are compared with Norouzbahari (2016),

[4] Awais, and Majeed (2013)[44] works as presented in Fig. 13. By increasing the CO_2 partial pressure, the enhancement factor for all three cases decreases linearly but not significant. In this figure, the Pz concentration and flow rate are 0.5 M and 1.5 l/h, respectively. It should be noted that the difference in the values of enhancement factor in this figure in comparison to our previous works[15,18,33] is at first in the difference in their operating conditions and second in the generality of this shape. Especially the diagram presented here is independent of the nanoparticle type.

To quantify the rate of absorption, the number of effective variables on computed enhancement factors is illustrated for the models presented in this work. However, the number of different parameters used in each model needs extra attention. Fig. 14 represents the alteration of the enhancement factor versus the film parameter (M) and a comparison of correlation and experimental data at different Pz concentrations. By increasing the Pz concentration, the enhancement factor increases. It means that the absorption process is
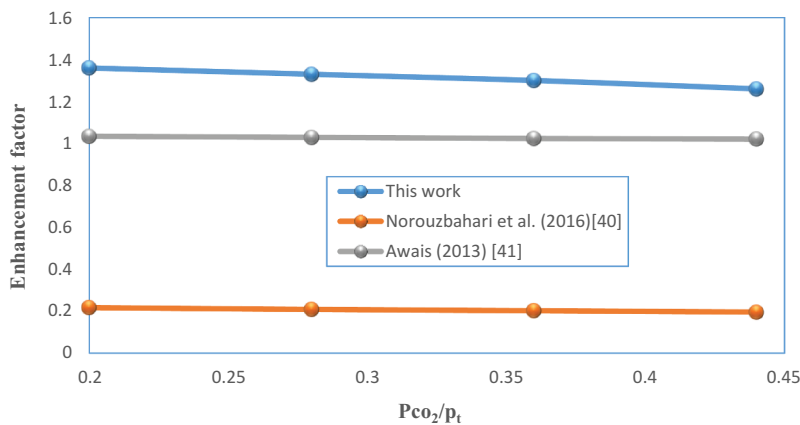

Fig. 13. Effects of CO_2 partial pressure on enhancement factor in different studies at Pz concentration of 0.5 M and flow rate of 1.5 l/h.
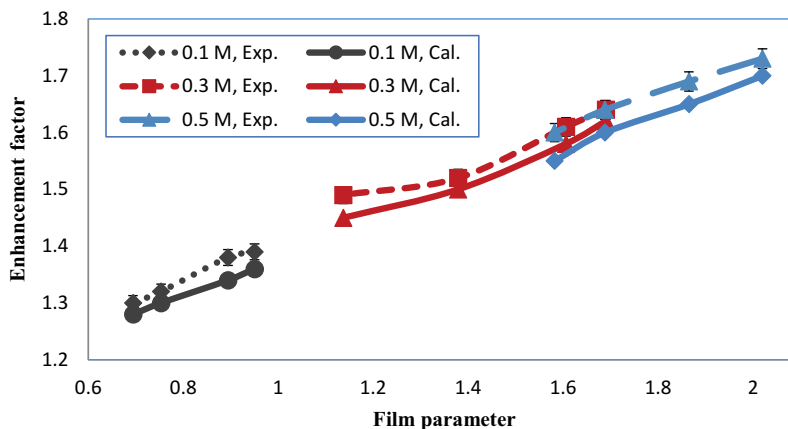

Figure 14. Comparison of experimental data and correlation for air-water-calcium alginate three-phase systems.
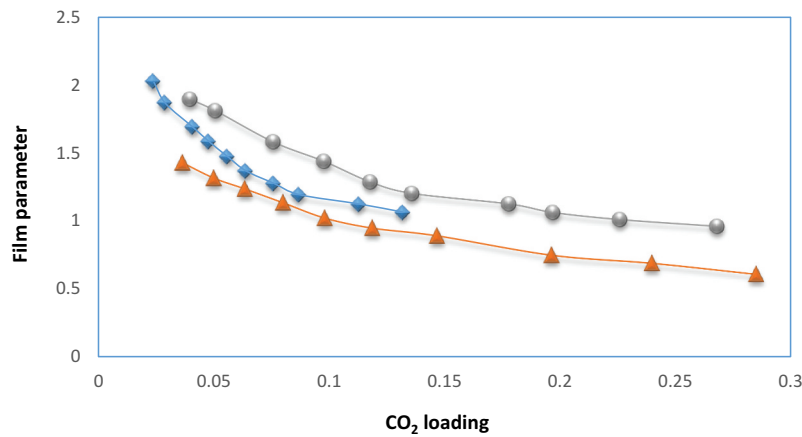
Fig. 15. Variation of CO_2 loading with the film parameter (this work).

performed faster at higher amine (*Pz*) concentration; this is clear because the difference in amine concentration (driving force) is proportional to the mass transfer flux.

Alterations of the CO_2 loading with the film parameter at three different *Pz* concentrations is shown in Fig. 15. The results indicate that at constant concentration, the solution with lower CO_2 loading has a more substantial film parameter (Hatta number). Furthermore, in constant loading, increasing concentration leads to an increase in the film parameter. Due to the power of the film parameter in Eq. (15) is negative, it causes to reduce the enhancement factor and finally the mass transfer flux. Due to the lower driving force at low concentrations, this decrease in the absorption rate is entirely expected due to the increase in concentration.

Conclusion

Since the CO_2 absorption industrial ranges are sufficiently comprehensive, having a model that covers broad ranges of operating conditions is of critical importance. In the present work, the Buckingham π theory with the dimensional analysis was developed to predict gas holdup, mass transfer coefficients, and enhancement factor in ternary H_2O- CO_2-*Pz* system, using experimental datasets reported in our previous work.[18] Some variable parameters, such as CO_2 partial pressure, apparent gas velocity, stirrer speed, and mass percentage of nanoparticles, were set as the input of the Buckingham theory. Furthermore, these parameters, including nanoparticle loading, film parameter, the ratio of CO_2 partial pressure to the total pressure, the film thickness of phases, CO_2 loading, and ratio of diffusion coefficients of CO_2 in gas and liquid phases were made dimensionless applying Buckingham π theory. The proposed correlation is a universal term and is appropriate for distinct

processes at various operating conditions. Also, another advantage of these relationships is that they can be used only for the base fluid or nanofluid. The consequences of the comparing the experimental data with the predictions, (%*AARD* = 3.78–18.14, *MSE* = 0–6.784 and R^2 = 0.861–0.980), specified that the Buckingham π theory has the potential to accurately predict of reactive absorption performance over a wide range of experimental conditions. The results showed that increasing the CO_2 load and CO_2 partial pressure had a negative effect on the enhancement factor. Also, the results indicated that with increasing *Pz* concentration and apparent gas velocity, the enhancement factor, and gas holdup was increased, respectively. A comparison of the result showed that the presented correlations are very accurate in contrast to the previous literature based on gas holdup, mass transfer coefficient, and enhancement factor.

Nomenclature

		p_{CO_2}	CO_2 partial pressure, Pa
AARD	Average Absolute Relative Deviation, %	P_t	Total pressure, Pa
C	Concentration, mol/l	*Pz*	Piperazine
Cal.	calculation	R^2	Coefficient of correlation
$C_{CO_2,b}$	carbon dioxide concentration in liquid bulk, mol/l	*Re*	Reynolds number
$C_{CO_2,i}$	carbon dioxide concentration in the gas-liquid interface, mol/l	*Sh*	Sherwood number
D_c	column diameter, m	*t*	Time, sec
Di	diffusion coefficient, m²/s	*T*	Temperature, K
E	Enhancement factor	u_g	gas velocity, m/s
Exp.	Experimental	u_G	apparent gas velocity, m/s
H	Liquid height, m	*we*	Webber number
k_{app}	apparent reaction rate constant,1/s	*X*	weight percent, %
k_g	gas film mass transfer coefficient, m/s	**Greek Letters**	

(Continued)

		p_{CO_2}	CO_2 partial pressure, Pa
AARD	Average Absolute Relative Deviation, %	P_t	Total pressure, Pa
C	Concentration, mol/l	Pz	Piperazine
Cal.	calculation	R^2	Coefficient of correlation
$C_{CO_2,b}$	carbon dioxide concentration in liquid bulk, mol/l	Re	Reynolds number
$C_{CO_2,i}$	carbon dioxide concentration in the gas-liquid interface, mol/l	Sh	Sherwood number
D_c	column diameter, m	t	Time, sec
Di	diffusion coefficient, m^2/s	T	Temperature, K
E	Enhancement factor	u_g	gas velocity, m/s
$Exp.$	Experimental	u_G	apparent gas velocity, m/s
H	Liquid height, m	we	Webber number
k_{app}	apparent reaction rate constant,1/s	X	weight percent, %
k_g	gas film mass transfer coefficient, m/s	**Greek Letters**	
K_G	Overall mass transfer coefficient, mol/ m^2.s. Pa	a_{CO_2}	CO_2 loading, mol CO_2/mol amine
k_l	liquid film mass transfer coefficient, m/s	ρ	Density, kg/m^3
M	film parameter	ε	Hold-up
MSE	Mean Squared Error	μ	Viscosity, kg/m.s
n_i	Absorbed mole, mole	σ	surface tension, N/m
N	stirrer speed, rpm	δ	film thickness, m
N_{CO_2}	Mass transfer flux, kmol/m^2.min		

ORCID

Ahad Ghaemi http://orcid.org/0000-0003-0390-4083

References

[1] Philippe Rekacewicz, U. G.-A.;.Availablefrom: http://wwwgridanoresources6362 .

[2] Pashaei, H.; Ghaemi, A.; Nasiri, M. Modeling and Experimental Study on the Solubility and Mass Transfer of CO_2 into Aqueous DEA Solution Using a Stirrer Bubble Column. *RSC Adv.* 2016, 6(109), 108075–108092. DOI: 10.1039/C6RA22589F.

[3] Norouzbahari, S.; Shahhosseini, S.; Ghaemi, A. Modeling of CO_2 Loading in Aqueous Solutions of Piperazine: Application of an Enhanced Artificial Neural Network Algorithm. *J. Nat. Gas Sci. Eng.* 2015, 24, 18–25. DOI: 10.1016/j.jngse.2015.03.011.

[4] Norouzbahari, S.; Shahhosseini, S.; Ghaemi, A. Chemical Absorption of CO_2 into an Aqueous Piperazine (PZ) Solution: Development and Validation of a Rigorous Dynamic Rate-based Model. *RSC Adv.* 2016, 6(46), 40017–40032.

[5] Rao, A. B.; Rubin, E. S. A Technical, Economic, and Environmental Assessment of Amine-based CO_2 Capture Technology for Power Plant Greenhouse Gas Control. *Environ. Sci. Technol.* 2002, 36(20), 4467–4475.

[6] Agency's, N.O.a.A.; Available from: http://www.noaa.gov/news/carbon-dioxide-levels-rose-at-record-pace-for-2nd-straight-year .

[7] Pashaei, H.; Ghaemi, A.; Nasiri, M. Experimental Investigation of CO_2 Removal Using Piperazine Solution in a Stirrer Bubble Column. Int. J. Greenhouse Gas Control. 2017, 63, 226–240.

[8] Naeem, S.; Ghaemi, A.; Shahhosseini, S. Experimental Investigation of CO_2 Capture Using Sodium Hydroxide Particles in a Fluidized Bed. *Korean J. Chem. Eng.* 2016, 33(4), 1278–1285.

[9] Freeman, S. A.; Dugas, R.; Van Wagener, D. H.; Nguyen, T.; Rochelle, G. T. Carbon Dioxide Capture with Concentrated, Aqueous Piperazine. *Int. J. Greenhouse Gas Con.* 2010, 4(2), 119–124.

[10] Nguyen, T.; Hilliard, M.; Rochelle, G. T. Amine Volatility in CO_2 Capture. *Int. J. Greenhouse Gas Con.* 2010, 4(5), p. p.707–715. DOI: 10.1016/j.ijggc.2010.06.003.

[11] Bougie, F.; Iliuta, M. C. CO2 Absorption in Aqueous Piperazine Solutions: Experimental Study and Modeling. *J. Chem. Eng. Data.* 2011, 56(4), 1547–1554. DOI: 10.1021/je1012247.

[12] Penders-van Elk, N. J.; Hamborg, E. S.; Huttenhuis, P. J.; Fradette, S.; Carley, J. A.; Versteeg, G. F. Kinetics of Absorption of Carbon Dioxide in Aqueous Amine and Carbonate Solutions with Carbonic Anhydrase. *Int. J. Greenhouse Gas Con.* 2013, 12, 259–268. DOI: 10.1016/j.ijggc.2012.10.016.

[13] Penders-van Elk, N. J.; Derks, P. W.; Fradette, S.; Versteeg, G. F. Kinetics of Absorption of Carbon Dioxide in Aqueous MDEA Solutions with Carbonic Anhydrase at 298K. *Int. J. Greenhouse Gas Con.* 2012, 9, 385–392. DOI: 10.1016/j.ijggc.2012.04.008.

[14] Bindwal, A. B.; Vaidya, P. D.; Kenig, E. Y. Kinetics of Carbon Dioxide Removal by Aqueous Diamines. *Chem. Eng. J.* 2011, 169(1–3), 144–150. DOI: 10.1016/j.cej.2011.02.074.

[15] Pashaei, H.; Ghaemi, A. CO2 Absorption into Aqueous Diethanolamine Solution with Nano Heavy Metal Oxide Particles Using Stirrer Bubble Column: Hydrodynamics and Mass Transfer. *J. Environ. Chem. Eng.* 2020, 8(5), 104110. DOI: 10.1016/j.jece.2020.104110.

[16] Bishnoi, S.; Rochelle, G. T. Absorption of Carbon Dioxide into Aqueous Piperazine: Reaction Kinetics, Mass Transfer and Solubility. *Chem. Eng. Sci.* 2000, 55(22), 5531–5543. DOI: 10.1016/S0009-2509(00)00182-2.

[17] Etemad, E.; Ghaemi, A.; Shirvani, M. Rigorous Correlation for CO_2 Mass Transfer Flux in Reactive Absorption Processes. *Int. J. Greenhouse Gas Con.* 2015, 42, 288–295. DOI: 10.1016/j.ijggc.2015.08.011.

[18] Pashaei, H.; Ghaemi, A.; Nasiri, M.; Heydarifard, M. Experimental Investigation of the Effect of Nano Heavy Metal Oxide Particles in Piperazine Solution on CO_2 Absorption Using a Stirrer Bubble Column. *Energy Fuels.* 2018, 32(2), 2037–2052.

[19] Bishnoi, S.; Rochelle, G. T. Absorption of Carbon Dioxide in Aqueous Piperazine/methyldiethanolamine. *AIChE J.* 2002, 48(12), 2788–2799. DOI: 10.1002/aic.690481208.

[20] Aroonwilas, A.; Veawab, A.; Tontiwachwuthikul, P. Behavior of the Mass-transfer Coefficient of Structured Packings in CO_2 Absorbers with Chemical Reactions. *Ind. Eng. Chem. Res.* 1999, 38(5), 2044–2050. DOI: 10.1021/ie980728c.

[21] Bougie, F.; Iliuta, M. C. CO_2 Absorption into Mixed Aqueous Solutions of 2-amino-2-hydroxymethyl-1,

3-propanediol and Piperazine. *Ind. Eng. Chem. Res.* 2009, 49(3), 1150–1159. DOI: 10.1021/ie900705y.

[22] Xu, G.; Zhang, C.; Qin, S.; Wang, Y. Kinetics Study on Absorption of Carbon Dioxide into Solutions of Activated Methyldiethanolamine. *Ind. Eng. Chem. Res.* 1992, 31(3), 921–927.

[23] Seo, D. J.; Hong, W. H. Effect of Piperazine on the Kinetics of Carbon Dioxide with Aqueous Solutions of 2-amino-2-methyl-1-propanol. *Ind. Eng. Chem. Res.* 2000, 39(6), 2062–2067. DOI: 10.1021/ie990846f.

[24] Ekerdt, J. G.; Freeman, B. D.; Schubert, C. *Thermodynamics and Kinetics of Aqueous Piperazine with Potassium Carbonate for Carbon Dioxide Absorption*, 2005.

[25] Derks, P.; Kleingeld, T.; Van Aken, C.; Hogendoorn, J. A.; Versteeg, G. F. Kinetics of Absorption of Carbon Dioxide in Aqueous Piperazine Solutions. *Chem. Eng. Sci.* 2006, 61(20), 6837–6854.

[26] Samanta, A.; Bandyopadhyay, S. Absorption of Carbon Dioxide into Aqueous Solutions of Piperazine Activated 2-amino-2-methyl-1-propanol. *Chem. Eng. Sci.* 2009, 64(6), 1185–1194. DOI: 10.1016/j.ces.2008.10.049.

[27] Servia, A.; Laloue, N.; Grandjean, J.; Rode, S.; Roizard, C. Modeling of the CO2 Absorption in a Wetted Wall Column by Piperazine Solutions. *Oil & Gas Science and Technology–Revue d'IFP Energies nouvelles.* 2014, 69(5), 885–902. DOI: 10.2516/ogst/2013136

[28] Safdar, R.; Thanabalan, M.; Omar, A. A. Solubility of CO_2 in 20 Wt.% Aqueous Solution of Piperazine. *Procedia Engineering.* 2016, 148, 1377–1379. DOI: 10.1016/j.proeng.2016.06.607.

[29] Dugas, R.; Rochelle, G. Absorption and Desorption Rates of Carbon Dioxide with Monoethanolamine and Piperazine. *Energy Procedia.* 2009, 1(1), 1163–1169. DOI: 10.1016/j.egypro.2009.01.153.

[30] Halim, H.; Shariff, A.; Bustam, M. High Pressure CO_2 Absorption from Natural Gas Using Piperazine Promoted 2-amino-2-methyl-1-propanol in a Packed Absorption Column. *Sep. Purif. Technol.* 2015, 152, 87–93. DOI: 10.1016/j.seppur.2015.08.004.

[31] Pashaei, H.; Ghaemi, A.; Nasiri, M.; Karami, B. Experimental Modeling and Optimization of CO_2 Absorption into Piperazine Solutions Using RSM-CCD Methodology. *ACS Omega.* 2020, 5(15), 8432–8448.

[32] Samanta, A.; Roy, S.; Bandyopadhyay, S. S. Physical Solubility and Diffusivity of N_2O and CO_2 in Aqueous Solutions of Piperazine and (N-methyldiethanolamine+ Piperazine). *J. Chem. Eng. Data.* 2007, 52(4), 1381–1385. DOI: 10.1021/je700083b.

[33] Heydarifard, M.; Pashaei, H.; Ghaemi, A.; Nasiri, M. Reactive Absorption of CO_2 into Piperazine Aqueous Solution in a Stirrer Bubble Column: Modeling and Experimental. Int. J. Greenhouse Gas Control. 2018, 79, 91–116.

[34] Van Der Spek, M.; Arendsen, R.; Ramirez, A.; Faaij, A. Model Development and Process Simulation of Postcombustion Carbon Capture Technology with Aqueous AMP/PZ Solvent. *Int. J. Greenhouse Gas Con.* 2016, 47, 176–199. DOI: 10.1016/j.ijggc.2016.01.021.

[35] Hughmark, G.;. Holdup and Mass Transfer in Bubble Columns. *Ind. Eng. Chem. Process Des. Dev.* 1967, 6(2), 218–220. DOI: 10.1021/i260022a011.

[36] Hikita, H.; Kikukawa, H. Liquid-phase Mixing in Bubble Columns: Effect of Liquid Properties. *Chem. Eng. J.* 1974, 8(3), 191–197. DOI: 10.1016/0300-9467(74)85024-0.

[37] Hikita, H.; Asai, S.; Tanigawa, K.; Segawa, K.; Kitao, M. Gas Hold-up in Bubble Columns. *Chem. Eng. J.* 1980, 20 (1), 59–67.

[38] Moshtari, B.; Babakhani, E. G.; Moghaddas, J. S. Experimental Study of Gas Hold-up and Bubble Behavior in Gas-liquid Bubble Column. *Pet. Coal.* 2009, 51(1), 27–32.

[39] Kumar, A.; Degaleesan, T. E.; Laddha, G. S.; Hoelscher, H. E. Bubble Swarm Characteristics in Bubble Columns. *Can. J. Chem. Eng.* 1976, 54(6), 503–508.

[40] Li, L.; Han, W.; Yu, H.; Tang, H. CO_2 Absorption by Piperazine Promoted Aqueous Ammonia Solution: Absorption Kinetics and Ammonia Loss. Greenhouse Gases: Sci. Technol.. 2013, 3(3), 231–245.

[41] Li, L.; Conway, W.; Puxty, G.; Burns, R.; Clifford, S.; Maeder, M.; Yu, H. The Effect of Piperazine (PZ) on CO_2 Absorption Kinetics into Aqueous Ammonia Solutions at 25.0°C. Int. J. Greenhouse Gas Control. 2015, 36, 135–143.

[42] Liu, J.; Wang, S.; Zhao, B.; Qi, G.; Chen, C. Study on Mass Transfer and Kinetics of CO_2 Absorption into Aqueous Ammonia and Piperazine Blended Solutions. *Chem. Eng. Sci.* 2012, 75, 298–308.

[43] Liu, J.; Wang, S.; Qi, G.; Zhao, B.; Chen, C. Kinetics and Mass Transfer of Carbon Dioxide Absorption into Aqueous Ammonia. *Energy Procedia.* 2011, 4, 525–532.

[44] Awais, M.;. Determination of the Mechanism of the Reaction between CO_2 and Alkanolamines. In *Institutt for Kjemisk Prosessteknologi.* 2013.

Appendix A A.1. Buckingham π theorem and gas holdup

There are various parameters, such as the liquid surface tension (σ_L), liquid viscosity (μ_L), gas density (ρ_G), inlet gas velocity (u_g), apparent gas velocity (u_G), the diameter of the bubble column reactor (D_c), CO_2 partial pressure at the inlet (P_{CO_2}), column pressure (P_t), liquid height (H_l), stirrer speed (N), the mass percentage of nanoparticles (X) which are affected the gas holdup. As can be seen, 12 active factors on gas holdup are specified, and the Buckingham π theorem is used to obtain a specific relationship. Based on this theorem, the gas holdup as a function of these factors is expressed as follows:

$$\varepsilon_G(\sigma_L, \mu_L, \rho_G, u_g, u_G, D_c, P_{CO_2}, P_t, H_l, N, X) = 0 \qquad \text{(A.1)}$$

Due to the number of primary variables, the number of dimensionless parameters is equal to (12–3 = 9). In this work, liquid density, apparent gas velocity, and column diameter are used as repetitive variables. Based on selected variables, the calculated dimensionless numbers for the gas holdup is presented in Table A.1.

The fifth and sixth dimensionless numbers were obtained in the following:

$$\pi_5 = \frac{P_{CO_2}}{\rho_G u_G^2}, \pi_6 = \frac{P_t}{\rho_G u_G^2}$$

By dividing the dimensionless number of π_5 to π_6, a new dimensionless number π_{new} is acquired. Therefore, one of the dimensionless numbers is decreased, and instead of eight numbers, seven dimensionless numbers were derived in this work.

$$\pi_{new} = \frac{\pi_5}{\pi_6} = \frac{P_{CO_2}}{P_t}$$

Ultimately, the final dimensionless numbers for the gas holdup phenomenon are given in the Appendix in Table B.1. The relationship of dimensionless numbers based on Buckingham π theorem is as follows:

$$\varepsilon_G = f(\pi_l, \pi_2, \pi_3, ..., \pi_7) \tag{A.2}$$

Using the dimensionless method of π-Buckingham, the dimensionless parameters of gas holdup are obtained in the following:

$$\varepsilon_G = f(\frac{H_l}{D_c}, \frac{\rho_G u_G D_c}{\mu_L}, \frac{\sigma_L}{\rho_G u_G^2 D_c}, \frac{u_g}{u_G}, \frac{P_{CO_2}}{P_t}, \frac{D_c N}{u_G}, X) \tag{A.3}$$

Finally, the relation between the obtained dimensionless numbers is:

$$\varepsilon_G = A(\frac{\rho_G u_G D_c}{\mu_L})^a (\frac{u_g}{u_G})^b (\frac{P_{CO_2}}{P_t})^c (\frac{\sigma_L}{\rho_G u_G^2 D_c})^d (\frac{H_l}{D_c})^e + f(\frac{D_c N}{u_G}) + g(X) \tag{A.4}$$

Coefficients of A, a, b, c . . . g are different depending on the operating parameters and problem conditions. By substituting the experimental values in Eq. (A.4), the gas holdup equation is determined using the data fitting method as follows:

$$\varepsilon_G = 2.3962 \times 10^{-5} \text{Re}^{-0.07841} we^{-4.75251}$$
$$(\frac{u_g}{u_G})^{0.002252} (\frac{P_{CO_2}}{P_t})^{0.155541} (\frac{H_l}{D_c})^{0.012}$$
$$+ 7.04 \times 10^{-8} (\frac{D_c N}{u_G}) + 0.206(X) \tag{A.5}$$

A.2. Buckingham π theorem and Mass transfer coefficients

In addition to the stated parameters in the previous section, the CO_2 diffusion coefficient in the Pz solution ($D_{CO2\text{-}Sol}$) affects the mass transfer coefficients. Hence, based on Buckingham π theorem, the mass transfer coefficient is a function of the mentioned parameters as follows:

$$K_G(\sigma_L, \mu_L, \rho_L, u_g, u_G, D_c, D_{CO_2-sol}, P_{CO_2}, P_t, H_l, N, X) = 0 \tag{A.6}$$

Due to the number of useful parameters, i.e., 13, the number of dimensionless numbers of the process for the mass transfer coefficient is equal to 10. Based on selected variables, calculated dimensionless numbers for the absorption system are represented in Table A.2.

Table 1.. Dimensionless numbers obtained in gas holdup.

Group	Dimensionless number	Group	Dimensionless number	Group	Dimensionless number	Group	Dimensionless number
π_1	$\rho_G^x u_G^y D_c^z H_L$	π_3	$\rho_G^x u_G^y D_c^z \sigma_L$	π_5	$\rho_G^x u_G^y D_c^z P_{CO_2}$	π_7	$\rho_G^x u_G^y D_c^z N$
π_2	$\rho_G^x u_G^y D_c^z \mu_L$	π_4	$\rho_G^x u_G^y D_c^z u_g$	π_6	$\rho_G^x u_G^y D_c^z P_t$	π_8	$\rho_G^x u_G^y D_c^z X$

Table 2.. Obtained dimensionless numbers in Mass transfer coefficients.

Group	Dimensionless number	Group	Dimensionless number	Group	Dimensionless number
π_1	$\pi_1 = \rho_G^x u_G^y D_c^z H_L$	π_4	$\pi_4 = \rho_G^x u_G^y D_c^z u_g$	π_7	$\pi_7 = \rho_G^x u_G^y D_c^z N$
π_2	$\pi_2 = \rho_G^x u_G^y D_c^z \mu_L$	π_5	$\pi_5 = \rho_G^x u_G^y D_c^z P_{CO_2}$	π_8	$\pi_8 = \rho_G^x u_G^y D_c^z X$
π_3	$\pi_3 = \rho_G^x u_G^y D_c^z \sigma_L$	π_6	$\pi_6 = \rho_G^x u_G^y D_c^z P_t$	π_9	$\pi_9 = \rho_G^x u_G^y D_c^z D_{CO_2-Sol}$

Table 3.. Obtained dimensionless numbers in Enhancement factor.

Group	Dimensionless number	Group	Dimensionless number	Group	Dimensionless number
π_1	$D_{CO_2-Sol}^x \delta_l^y C_{CO_2}^z N_A$	π_4	$D_{CO_2-Sol}^x \delta_l^y C_{CO_2}^z \delta_G$	π_7	$D_{CO_2-Sol}^x \delta_l^y C_{CO_2}^z C_{Pz}$
π_2	$D_{CO_2-Sol}^x \delta_l^y C_{CO_2}^z k_{app}$	π_5	$D_{CO_2-Sol}^x \delta_l^y C_{CO_2}^z P_{CO_2}$	π_8	$D_{CO_2-Sol}^x \delta_l^y C_{CO_2}^z N$
π_3	$D_{CO_2-Sol}^x \delta_l^y C_{CO_2}^z D_{CO_2-gas}$	π_6	$D_{CO_2-Sol}^x \delta_l^y C_{CO_2}^z P_t$	π_9	$D_{CO_2-Sol}^x \delta_l^y C_{CO_2}^z X$

Table 4. The error percentage and correlation coefficient for the presented correlations.

Correlation	RMSEP	R^2	AARD%
Gas holdup	2.604	0.861	8.79
Total mass transfer coefficient	0.313	0.952	12.82
Mass transfer coefficient in gas phase	0.021	0.980	4.53
Mass transfer coefficient in liquid phase	0.472	0.972	18.14
Enhancement factor	0.095	0.980	3.78

The *RMSEP*, R^2, and *AARD* accuracy are 0.001, 0.001, and 0.01, respectively.

In this work, the liquid density, the apparent gas velocity, and the column diameter are also used as repetitive variables. Also, the selected primary variables are the same as the previous section. In this case, a new dimensionless group of $\rho_G^x u_G^y D_c^z D_{CO_2-Sol}$ is added the dimensionless numbers of gas holdup, which is presented in Table 4. In this section, the new dimensionless number, π_{new}, is obtained from dividing the dimensionless number of π_5 to π_6 as a previous section and decreased the dimensionless numbers from 9 to 8. The ratio of diffusion coefficient to apparent gas velocity, i.e., $\frac{D_{CO_2-Sol}}{u_G D_c}$, is now added to the presented number in Table B.1. Thus, the function of mass transfer coefficients using Buckingham π theorem is in the following:

$$K_G = f\left(\frac{H_l}{D_c}, \frac{\rho_L u_G D_c}{\mu_L}, \frac{\sigma_L}{\rho_G u_G^2 D_c}, \frac{u_g}{u_G}, \frac{P_{CO_2}}{P_t}, \frac{D_c N}{u_G}, \frac{D_{CO_2-sol}}{u_G D_c}, X\right)$$

(A.7)

The relationship between dimensionless numbers for mass transfer coefficients is determined as given:

$$K_G = A\left(\frac{\rho_L u_G D_c}{\mu_L}\right)^a \left(\frac{u_g}{u_G}\right)^b \left(\frac{P_{CO_2}}{P_t}\right)^c \left(\frac{\sigma_L}{\rho_G u_G^2 D_c}\right)^d \left(\frac{D_{CO_2-sol}}{u_G D_c}\right)^e$$
$$+ f\left(\frac{D_c N}{u_G}\right) + g(X)$$

(A.8)

By substituting the experimental data and data fitting method, the equations of mass transfer coefficients are determined as below:

$$K_G = 5.127 \times 10^{-5} \text{Re}^{-0.09471} we^{0.04126}$$
$$\left(\frac{u_g}{u_G}\right)^{-0.02478} \left(\frac{P_{CO_2}}{P_t}\right)^{0.060279} \left(\frac{H_l}{D_c}\right)^{0.012} \times \left(\frac{D_{CO_2-sol}}{u_G D_c}\right)^{-0.0133}$$
$$- 1.81 \times 10^{-6}\left(\frac{D_c N}{u_G}\right)^{0.000331} - 2.326 \times 10^{-4}(X)$$

(A.9)

$$k_g = 4.814 \times 10^{-4} \text{Re}^{-0.3471} we^{0.04126}$$
$$\left(\frac{u_g}{u_G}\right)^{-0.01478} \left(\frac{P_{CO_2}}{P_t}\right)^{-1.240279} \left(\frac{H_l}{D_c}\right)^{0.012} \times \left(\frac{D_{CO_2-sol}}{u_G D_c}\right)^{-0.0133}$$
$$- 1.3 \times 10^{-6}\left(\frac{D_c N}{u_G}\right)^{0.00311} - 2.326 \times 10^{-4}(X)$$

(A.10)

$$k_l = 5.167 \times 10^{-5} \text{Re}^{-0.08671} we^{0.04126}$$
$$\left(\frac{u_g}{u_G}\right)^{-0.003442} \left(\frac{P_{CO_2}}{P_t}\right)^{-0.059279} \left(\frac{H_l}{D_c}\right)^{0.012} \times \left(\frac{D_{CO_2-sol}}{u_G D_c}\right)^{-0.0133}$$
$$- 1.81 \times 10^{-6}\left(\frac{D_c N}{u_G}\right)^{0.000331} - 2.326 \times 10^{-4}(X) wt\%0.01$$

(A.11)

A.3. Buckingham π theorem and Enhancement factor

The valid parameters and factors on mass transfer flux are given in equation as below:

$$N_A(k_{app}, D_{CO_2-sol}, D_{CO_2-gas}, \delta_g, \delta_l, P_{CO_2}, P_t, C_{CO_2}, C_{Pz}, N, X)$$
$$= 0$$

(A.12)

Since the number of valid parameters is equal to 12, the number of dimensionless numbers will be 9. The selected primary variables in this case are C_{CO_2}, δ_l, and $D_{CO_2,Sol}$. Based on selected variables, calculated dimensionless numbers for the absorption system are represented in Table B.3.

By calculating the coefficients of the groups, the dimensionless numbers are obtained, as expressed in Eq. (A.13) (see appendix B). The relationship between dimensionless numbers, in this case, is as follows:

$$E = \frac{N_{CO_2}}{k_l C_{CO_2}}$$
$$= A(Sh)^a (\alpha)^b (M)^c \left(\frac{P_{CO_2}}{P_t}\right)^d \left(\frac{\delta_g}{\delta_l}\right)^e \left(\frac{D_{CO_2-gas}}{D_{CO_2-Pz}}\right)^f + g\left(\frac{\delta_l^2 N}{D_{CO_2-Pz}}\right)$$
$$+ h(X)$$

(A.13)

The coefficients of A, a, b ... h are obtained using experimental data substitution and data fitting methods. Thus, the enhancement factor equation is generated as follows:

$$E = 11.56 Sh^{0.9037} (\alpha)^{0.023} (M)^{-0.0102} \left(\frac{P_{CO_2}}{P_t}\right)^{-0.0356} \left(\frac{\delta_g}{\delta_l}\right)^{-0.0191}$$
$$\times \left(\frac{D_{CO_2-gas}}{D_{CO_2-sol}}\right)^{-0.5024} - 0.005\left(\frac{\delta_l^2 N}{D_{CO_2-sol}}\right) - 0.0009(X)$$

(A.14)

The fifth and sixth dimensionless numbers (see Table B.3) were obtained in the following:
$$\pi_5 = \frac{\delta_l P_{CO_2}}{D_{CO_2-Sol} C_{CO_2}^2}, \pi_6 = \frac{\delta_l P_t}{D_{CO_2-Sol} C_{CO_2}^2}$$
By dividing the dimensionless number of π_5 to π_6, a new dimensionless number π_{new} is acquired. Therefore, one of the dimensionless numbers is decreased, and instead nine numbers, eight dimensionless numbers were derived in this work.

$$\pi_{new} = \frac{P_{CO_2}}{P_t}$$

Appendix B

Table 1. Definition of obtained dimensionless numbers using Buckingham π theorem.

Num.	Definition of dimensionless number	Dimensionless number
1	Ratio of liquid height in column to internal diameter of column	$\frac{H_l}{D_c}$
2	Reynolds number: indicates ratio of inertial force to viscous force	$\frac{\rho_G u_G D_c}{\mu_L}$
3	Weber number: ratio of surface tension force to Inertia force	$\frac{\sigma_L}{\rho_G u_G^2 D_c}$
4	Ratio of inlet gas velocity to apparent gas velocity	$\frac{u_g}{u_G}$
5	Ratio of CO_2 partial pressure in gas phase to total pressure	$\frac{P_{CO_2}}{P_t}$
6	Ratio of stirrer speed to apparent gas velocity	$\frac{D_c N}{u_G}$
7	Weight percentage of nanoparticles	X
8	Ratio of diffusion coefficient of CO_2 in liquid phase to apparent gas velocity	$\frac{D_{CO_2-Sol}}{u_G D_c}$
9	Enhancement factor: ratio of absorption rate with chemical reaction to one without chemical reaction	$E = \frac{N_A}{\delta_l D_{CO_2-Pz} C_{CO_2}} = \frac{N_A}{k_l C_{CO_2}}$
10	Film parameter: ratio of maximum film conversion in film to maximum diffusion rate through the film	$M = \frac{k_{app} \delta_l^2}{D_{CO_2-Pz}}$
11	Loading: ration of absorbed concentration of CO_2 to amine concentration in circulation	$a = \frac{C_{CO_2}}{C_{Pz}}$
12	Ratio of gas film thickness to liquid film thickness	$\frac{\delta_g}{\delta_l}$
13	Ratio of diffusion coefficient of CO_2 in gas phase to one in liquid phase	$\frac{D_{CO_2-gas}}{D_{CO_2-Pz}}$
14	Ratio of stirrer speed to diffusion coefficient of CO_2 in solution	$\frac{\delta_l^2 N}{D_{CO_2-Pz}}$